Progress in Fractional Differentiation and Applications
An International Journal

http://dx.doi.org/10.18576/pfda/080211

Conformable derivative: A derivative associated to the Riemann-Stieltjes integral

Abdon Atangana[1,2], *Ali Akgül*[3,*], *Muhammad Altaf Khan*[1] *and Rabha Waell Ibrahim*[4]

[1] Institute for Groundwater Studies, Faculty of Natural and Agricultural Science, University of Free State, 9300, Bloemfontein, South Africa
[2] Department of Medical Research, China, Medical University Hospital, China, Medical University, Taichung, Taiwan
[3] Siirt University, Art and Science Faculty, Department of Mathematics, TR-56100 Siirt, Turkey
[4] IEEE: 94086547, Kuala Lumpur, 59200, Malaysia

Received: 2 Sep. 2021, Revised: 18 Oct. 2021, Accepted: 20 Jan. 2022
Published online: 1 Apr. 2022

Abstract: In mathematics, the Riemann-Stieltjes integral $\int f(t)dg(t)$ is known to be the more general version of the well-known Riemann integral that is used in classical integral calculus. This integral has found application in several fields. However, there is no clear derivative associate to the generalized integral, except the concept of global derivative that was suggested very recently. Nevertheless, a more generalized differential operator called conformable derivative was suggested and many concerns have been raised as what such operator cannot be considered as derivative. In this paper, we proved that not only the operator is a derivative but a derivative associate to the well-known Riemann-Stieltjes integral. We have in addition present some applications of the conformable derivative in image processing and dynamical processes including chaos and epidemiology.

Keywords: Conformable derivative, Stieltjes integral, image processing, chaos, fractal calculus, and epidemiology.

1 Introduction

One of the main concerns of humans is to evaluate changes occurring in nature. Their concern is to know either there is a positive, constant or negative changes, this information help them to project what could possibly happen in future. The reason behind this aim is to be in perfect control of their environment. They usually follow several steps to achieve their goal, the first one require collected of data, or observation of a specific process behavior for a short or long period. The second is step is analysis of collected data and remove of uncertainties to have data that represent the real world scenario. The last time is the conversion of observed facts into mathematical models, which will further be solved to see the future behaviors of the process. The last steps has attracted attention of many scholars from different background. The concept of differentiation is used to construct these mathematical models. The concept of differentiation originated from the formula of rate of change. Let f be a continuous function between point a and b then the rate of change is a value

$$r = \frac{f(b) - f(a)}{b - a}.$$

If the value is positive, we can say that there is a positive change or increase, if the value is zero, we can conclude there is no change, finally if the value is negative, we can conclude that there is a negative change or a decrease. However if

$$\lim_{b \to a} \frac{f(b) - f(a)}{b - a}.$$

exists, we can conclude that the function has a derivative at the point a, thus in general by taking any point within the domain of the function f if the following limit exists

$$\lim_{h \to 0} \frac{f(x+h) - f(x)}{h},$$

* Corresponding author e-mail: aliakgul00727@gmail.com

then,

$$\lim_{h\to 0}\frac{f(x+h)-f(x)}{h}=f'(x)$$

is called the derivative of the function f. One of the real world problem that the above can describe is:

$$v(t)=\lim_{t\to t_0}\frac{x(t)-x(t_0)}{t-t_0}$$

which is known as instantaneous velocity. Another important concept that depend on the rate of change is the acceleration

$$ac=\frac{dv(t)}{dt}.$$

Many important quantities depend on the rate of change including the kinetic energy of a moving object

$$E_{kenetic}=\frac{1}{2}mv^2.$$

The momentum which is a vector defined by the following equation

$$p=mv.$$

The Lorenz factor defined as

$$\gamma=\frac{1}{\sqrt{1-\frac{v^2}{c^2}}}.$$

The quantity derivative was used to form an ordinary differential equation, where there is one variable, a partial differential equation where more than one parameter. These two classes of differential equations have formed sub-topics in mathematics and applied mathematics; they have been used in modeling real world problems with no memory with some success and limitations.

Recently, it has been established that numerous models in science and engineering can be demonstrated additional perfectly by arbitrary derivatives (fractional calculus, conformable calculus (CC) and fractal) than normal derivatives, and various approaches are settled to resolve the issue of analysis. Due to the additional unrestricted fractional power, approaches deliver supplementary degree of freedom in optimization presentation. Unexpectedly, various conformable calculus approaches have been utilized in image processing field. Here current studies are reviewed in different sub-fields, which contain image enhancement, image edge detection, image denoising, image segmentation, image registration, image fusion, image recognition, image encryption, image compression and image restoration. In sum, it is well demonstrated that as an essential mathematic implement, CC displays unlimited achievement in image processing.

2 Associated integral

Here, we present the integral associated to conformable derivatives. We have already showed above that such integral is a particular case of the well known Riemann–Stieltjes integral. Here, we present how such integral is obtained using fundamental theorem of calculus. Let us consider the following equation.

$$\begin{aligned}&T_t^{\alpha}y(t)=u(t),\quad t>0,\\&y(0)=y_0.\end{aligned}$$

We assume that $y(t)$ is differentiable such that

$$\begin{aligned}&\frac{dy(t)}{dt}=t^{\alpha-1}u(t),\quad t>0,\\&y(0)=y_0.\end{aligned}$$

Applying the integral on both sides yields

$$y(t)-y(0)=\int_0^t\tau^{\alpha-1}u(\tau)d\tau,\quad t>\tau>0.$$

The above infers that

$$ {}^{\alpha}I_t f(t) = \int_0^t \tau^{\alpha-1} f(\tau) d\tau = \int_0^t f(\tau) d\left(\frac{\tau^\alpha}{\alpha}\right) = \int_0^t f(\tau) dg(\tau), $$

which is indeed the Riemann–Stieltjes integral with $g(\tau) = \frac{\tau^\alpha}{\alpha}$. By defining the following infinite norm $\|\phi\|_\infty = \sup_{t\in D_\phi} |\phi(t)|$, we get

$$ \begin{aligned} {}^{\alpha}I_t f(t) \leq |{}^{\alpha}I_t f(t)| &= \left| \int_0^t \tau^{\alpha-1} f(\tau) d\tau \right| \\ &\leq \int_0^t \tau^{\alpha-1} |f(\tau)| d\tau < \int_0^t \tau^{\alpha-1} \sup_{l\int[0,\tau]} |f(l)| d\tau \\ &< \sup_{t\int[0,T]} |f(t)| \frac{t^\alpha}{\alpha} < \|f\|_\infty \frac{T^\alpha}{\alpha}. \end{aligned} $$

and

$$ \begin{aligned} |{}^{\alpha}I_t f(t) - {}^{\alpha}I_t g(t)| &= \left| \int_0^t \tau^{\alpha-1} (f(\tau) - g(\tau)) d\tau \right| \\ &\leq \int_0^t \tau^{\alpha-1} |f(\tau) - g(\tau)| d\tau \\ &\leq \int_0^t \tau^{\alpha-1} \sup_{l\in[0,\tau]} |f(l) - g(l)| d\tau \\ &\leq \sup_{t\in[0,T]} |f(t) - g(t)| \frac{t^\alpha}{\alpha} \\ &\leq \|f - g\|_\infty \frac{T^\alpha}{\alpha}. \end{aligned} $$

If f is positive on $[0,T]$, then $\int_0^t f(\tau) d\frac{\tau^\alpha}{\alpha}$ can be viewed as the surface under the curve of $f(t)$ and above the function $\frac{t^\alpha}{\alpha}$. Since $0 < \alpha < 1$, $\left(\int_0^t f(\tau) d\frac{\tau^\alpha}{\alpha}\right)_{\alpha\in(0,1)}$ is a family of surface under the curve $f(t)$ and the above curve $\frac{t^\alpha}{\alpha}$. Indeed the conformable integral admits an integration by parts in the form

$$ \int_a^b f(t) d\frac{t^\alpha}{\alpha} = f(b)\frac{b^\alpha}{\alpha} - f(a)\frac{a^\alpha}{\alpha} - \int_0^t \frac{t^\alpha}{\alpha} df(t). $$

For example if $f(t) = t$, we have

$$ \int_a^b t d\left(\frac{t^\alpha}{\alpha}\right) = \frac{b^{\alpha+1}}{\alpha} - \frac{a^{\alpha+1}}{\alpha} - \left(\frac{b^{\alpha+1}}{\alpha+1} - \frac{a^{\alpha+1}}{\alpha+1}\right) = \frac{b^{\alpha+1}}{\alpha}\left(1 - \frac{1}{\alpha+1}\right) + \frac{a^{\alpha+1}}{\alpha}\left(\frac{1}{\alpha+1} - 1\right). $$

Following Gerber and coauthors it has been showing that the Cavalieri principle can easily be employed to determine areas or family of area bounded by curves using conformable derivatives. This achieve this one needs to have the integrations strips Riemann integration substituted by strips which are non-rectangular in form. The aim being to transform a Cavalieri region with a transformation ξ, or perhaps use $\frac{t^\alpha}{\alpha} = \xi^{-1}$ as integrand.

3 Motivation

To complete the calculus, corresponding integral was associated to this concept and was obtained as

$$ {}_a^b I f(t) = \int_a^b f(t) dt. \tag{1} $$

A direct interpolation was given to the above formula is the area under the curve of $f(t)$ if f is positively defined. A link between differential and integral calculus was established via fundamental theorem of calculus.

$$\int_a^t f'(\tau)d\tau = f(t) - f(a) \tag{2}$$

$$\frac{d}{dt}\int_a^t f(\tau)d\tau = f(t). \tag{3}$$

This concept can be traced back to works done by Greek Eudoxus who was determining the areas and volumes by breaking them up into an infinite number of divisions for which the volumes and areas are well known. The second is methodology was extended by Archimedean and was used to determine area of a circle, the surface area, volume of sphere, surface of sphere, surface of an ellipse, the surface under a parabola, the surface of a spiral, and many other quantities. However it is worth nothing that, in early $17th$ century, a significant step was made to connect differential and integral calculus, this was achieved by Barrow and Torricelli. On a serious not, the initial proof of the fundamental theorem of calculus was provided by Barrow. Nonetheless, a major contribution was done indecently by Leibnitz and Newton as they provided insight of the fundamental theorem of calculus. It is documented in the literature that the first term was introduced by Leibnitz in 1675, where he adopted the symbol $\int$. On the other hand the notion used by Newton was to ambiguous and could not be adopted. The literature has documented several different definitions of integrals. We can list the Darboux integral, the Rieamnn-Stieltjes integral, Lebesgue-Stieltjes integral, the Daniell integral, the Haar integral, the Henstock–Kurzweil integral, the Ito integral, Choquet integral and others.

While we have listed several important integral that were named after their funders, we will focus on the Rieamnn-Stieltjes integral. This integral was named after Bernhard Riemann and Thomas Joannes Stieltjes. It is documented that the definition was first published in 18994 by Thomas Joannes Stieltjes. The integral has many applications in real world, for example statistic and continuous probability. The Rieamnn-Stieltjes integral of a function f on $[a,b]$ with respect to another real-to-real function g is denoted by $\int_a^d f(x)dg(x)$. This integral is more general than classical version. For example, if $g(x) = x$ we recover $\int_a^b f(x)dx$. If $a = -\infty$, $b = \infty$ and $g(x)$ is differentiable, we get

$$\int_{-\infty}^{\infty} f(x)g'(x)dx = E(\delta(x)), \tag{4}$$

which is an expected value for g which is considered now as the cumulative probability distribution of a random variable. In general if $g(x)$ is differentiable, we have

$$\int_a^b f(x)dg(x) = \int_a^b f(x)g'(x)dx. \tag{5}$$

Thus, if the upper boundary is t, we have

$$\int_0^t f(x)dg(x) = \int_0^t f(x)g'(x)dx. \tag{6}$$

From the above well-known and applied integral if $g(x) = \frac{x^\alpha}{\alpha}$, then

$$\int_0^t f(x)dg(x) = \int_0^t f(x)x^{\alpha-1}dx, \tag{7}$$

where $\alpha > 0$ and $x > 0$. By solving the following equation

$$\int_0^t f(x)x^{\alpha-1}dx = u(t), \tag{8}$$

we get

$$f(t)t^{\alpha-1} = u'(t). \tag{9}$$

and

$$f(t) = u'(t)t^{1-\alpha}. \tag{10}$$

If u is differentiable, then we have

$$f(t) = \lim_{h\to 0}\frac{u(t+h)-u(t)}{h}t^{1-\alpha}. \tag{11}$$

Replacing $h = \varepsilon t^{1-\alpha}$, we get

$$f(t) = \lim_{\varepsilon \to 0} \frac{u(t + \varepsilon t^{1-\alpha}) - u(t)}{\varepsilon}. \tag{12}$$

The above formula is nothing else than the well-known conformable derivative. Owing the fact that the Rieamnn-Stieltjes integral form a general calculus used for more complex problem, for example volumes. The Riemann integral being a particular case of the Rieamnn-Stieltjes, make us calculus that the conformable derivative is clearly a more generalized classical derivative. If $g(t) = t^{\alpha}$, then we obtain

$$J_t^{\alpha} f(t) = \alpha \int_0^t \tau^{\alpha-1} f(\tau) d\tau. \tag{13}$$

We solve the following equation

$$J_t^{\alpha} f(t) = u(t), \tag{14}$$

where u is differentiable. Then, we obtain

$$\alpha t^{\alpha-1} f(t) = u'(t) \tag{15}$$

and

$$f(t) = \frac{u'(t)}{\alpha t^{\alpha-1}}. \tag{16}$$

u being differentiable leads to

$$f(t_1) = \frac{\lim_{t \to t_1} \frac{u(t) - u(t_1)}{t - t_1}}{\lim_{t \to t_1} \frac{t^{\alpha} - t_1^{\alpha}}{t - t_1}}. \tag{17}$$

Then, we obatin

$$f(t_1) = \lim_{t \to t_1} \frac{u(t) - u(t_1)}{t^{\alpha} - t_1^{\alpha}}, \tag{18}$$

which is the well-known fractal derivative.

One of the main motivation to introduce the conformable derivative was that fractional derivatives do not satisfy Leibniz law and other properties hold by classical differential operator. This argument was not valid due to the difference between classical derivative and fractional differential operators. One of the principal difference is that fractional is convolution of classical derivative with different kernels. It is therefore impossible for these operators to satisfy laws of classical mechanic. These properties are not prerequisites for an operator to be considered as derivative. However, the operator was defined as follow [22]:

$$T_t^{\alpha} f(t) = \lim_{\varepsilon \to 0} \frac{f(t + \varepsilon t^{1-\alpha}) - f(t)}{\varepsilon}. \tag{19}$$

The definition covers a large class of function that are not necessary differentiable only the above limit need to exist on a particular note. However, if the function is differentiable, one can convert the definition to, by letting $\varepsilon t^{1-\alpha} = h$,

$$T_t^{\alpha} f(t) = \lim_{h \to 0} \frac{f(t + h) - f(t)}{h t^{\alpha-1}} = f'(t) t^{1-\alpha}. \tag{20}$$

On the other hand, if we put

$$\frac{1}{t^{1-\alpha}} = \lim \frac{t_1^{\alpha} - t^{\alpha}}{t_1 - t} \frac{1}{\alpha}. \tag{21}$$

Therefore, the conformable derivative can be reformulated as:

$$\lim_{t_1 \to t} \frac{f(t_1) - f(t)}{t_1 - t} \frac{\alpha}{\frac{t_1^{\alpha} - t^{\alpha}}{t_1 - t}} = \frac{f(t_1) - f(t)}{t_1^{\alpha} - t^{\alpha}} \alpha, \tag{22}$$

where $\alpha > 0$. Therefore, we reach

$$\lim_{t_1 \to t} \frac{f(t_1) - f(t)}{\frac{t_1^\alpha}{\alpha} - \frac{t^\alpha}{\alpha}}. \tag{23}$$

The above formula therefore shows that the conformable derivative is the limit of the rate of change of the function f with respect to the function $g(t) = \frac{t^\alpha}{\alpha}$. If $\alpha = 1$, we indeed cover

$$\lim_{t_1 \to t} \frac{f(t_1) - f(t)}{t_1 - t} = f'(t). \tag{24}$$

Properties of this operator are well presented in [22], where the concept was introduced. However, this operator has one property that for some researchers it is a weakness or a point that disqualifies the operator to be called a derivative. However, a deeper analysis made in [22] suggested that such property makes the operator more suitable to model complex system with crossover behaviours. For reader that are not aware of this, we note here the property. Let $0 < \alpha, \beta \leq 1$.

$$T_t^{\alpha+\beta} f(t) \neq T_t^\alpha f(t) \left[T_t^\beta f(t)\right] \neq T_t^\beta f(t) \left[T_t^\alpha f(t)\right]. \tag{25}$$

Why such is strength than a weakness? The answer relies on Atangana-Gomez bracket. If f is a function such that $D^{\alpha+\beta} f$ and $D^\alpha \left(D^\beta f\right)$ exists, if $D^\alpha \left(D^\beta f\right) \neq D^\beta \left(D^\alpha f\right)$, then the operator is able to perform crossover behaviours, if not no crossover behaviours can be performed by the operator. And indeed for the conformable derivative, when $\alpha = 1$, we have that

$$T_t[T_t f] = T_{t^2}^2 f. \tag{26}$$

Then, their Atangana-Gomez bracket is zero, meaning the classical differential operator can not predict crossover behaviours. However, if $\alpha \neq \beta \in (0,1)$, we have that

$$T_t^\alpha [T_t^\beta f] \neq T_t^\beta [T_t^\alpha f], \tag{27}$$

which means their Atangana-Gomez bracket is nonnull. This means the conformable derivative can predict crossover behaviours. Already Nieto, Sachin and other have demonstrated that the nonlocal operators do not satisfy index law. In particular, Sachin and his coauthors proved that when index law is satisfied produce only trivial solutions. We underpin our discussion with the following example.

$$\frac{dy(t)}{dt} = -\lambda y(t),$$
$$y(0) = y_0,$$

and

$$T_t^\alpha y(t) = -\lambda y(t),$$
$$y(0) = y_0.$$

We have exact solutions as:

$$y(t) = y_0 \exp(-\lambda t)$$

and

$$y(t) = y_0 \exp\left(-\lambda \frac{t^\alpha}{\alpha}\right),$$

respectively.

The solution of classical model provides a simple exponential function. On the other hand, the solution of the other model provides stretched exponential. Numerical solutions are provided below. It is clear from the plots one can conclude that solution from conformable provides a solution that is more realistic in terms of complexity.

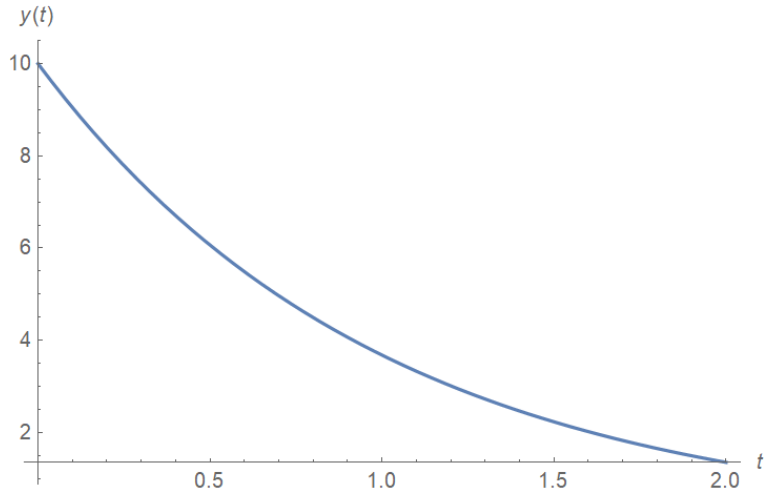

Fig. 1: Simulation of the solution of the classical problem.

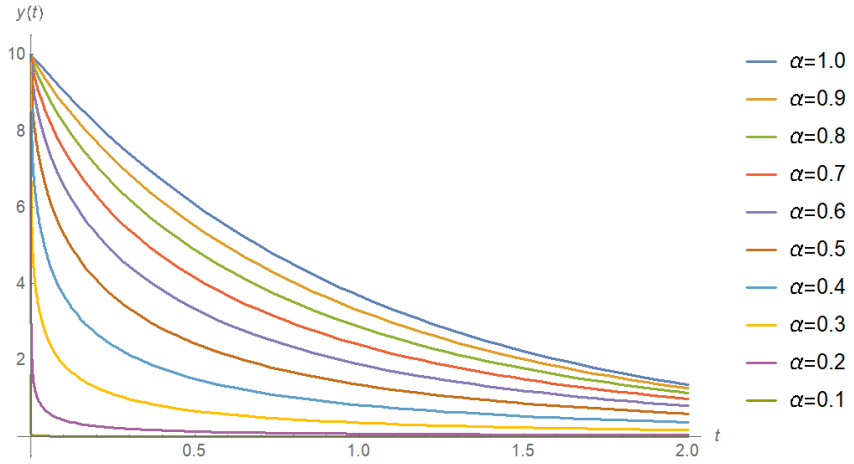

Fig. 2: Simulation of the solution for different values of α at $\lambda = 1$ and $y_0 = 10$.

Classical ordinary and partial differential equations with variable coefficients, have been documented to be more suitable to modelling complex real world problems unlike those with constant coefficients. It should be noted that, replacing classical time or spacial derivative with confirmable, leads to differential equation with variable coefficients. To show this, we consider a well-known partial differential equations.

$$\frac{\partial c(x,t)}{\partial t} = -V\frac{\partial c(x,t)}{\partial x} + \frac{\partial^2 c(x,t)}{\partial x^2}. \tag{28}$$

We replace time and spacial derivative by conformable

$$T_t^{\alpha} c(x,t) = -V T_x^{\alpha} c(x,t) + T_x^{\alpha}\left(T_x^{\alpha} c(x,t)\right). \tag{29}$$

Since in this case $c(x,t)$ is twice differentiable in space and differentiable in time, we have that

$$T_t^{\alpha} c(x,t) = \frac{\partial c(x,t)}{\partial t}\frac{1}{t^{\alpha-1}}, \tag{30}$$

$$T_x^{\alpha} c(x,t) = \frac{\partial c(x,t)}{\partial x} \frac{1}{x^{\alpha-1}}, \tag{31}$$

$$T_x^{\alpha}\left(T_x^{\alpha} c(x,t)\right) = \frac{1}{x^{\alpha-1}}\left((1-\alpha)x^{-\alpha}\frac{\partial c(x,t)}{\partial x} + x^{1-\alpha}\frac{\partial^2 c(x,t)}{\partial x^2}\right),$$
$$= (1-\alpha)x^{1-2\alpha}\frac{\partial c(x,t)}{\partial x} + x^{2-2\alpha}\frac{\partial^2 c(x,t)}{\partial x^2}.$$

Replacing in the original equation yields

$$\frac{\partial c(x,t)}{\partial t} = -Vt^{\alpha-1}\left(x^{1-\alpha} + (1-\alpha)x^{1-2\alpha}\right)\frac{\partial c(x,t)}{\partial x},$$
$$+Dt^{\alpha-1}x^{2-2\alpha}\frac{\partial^2 c(x,t)}{\partial x^2}.$$

Put $V(x,t) = Vt^{\alpha-1}\left(x^{1-\alpha} + (1-\alpha)x^{1-2\alpha}\right)$ and $D(x,t) = Dt^{\alpha-1}x^{2-2\alpha}$. Then, we get

$$\frac{\partial c(x,t)}{\partial t} = -V(x,t)\frac{\partial c(x,t)}{\partial x} + D(x,t)\frac{\partial^2 c(x,t)}{\partial x^2}.$$

This produces a family of advection dispersion equations, where velocity coefficient is a function of α, x and t, then name with the dispersion coefficients. Thus family of advection family equations is able to describe solid movement normal, super and slow flow, behaviours that are found in real world situations. $D(x,t)$ provides super dispersion, slow and normal dispersion. We shall present derivation of numerical solution of such advection-dispersion equation. At the point (x_i,t_n), we have

$$\frac{c_i^{n+1} - c_i^n}{\Delta t} = -V(x_i,t_n)\frac{c_{i+1}^n - c_{i-1}^n}{2\Delta x}, +D(x_i,t_n)\frac{c_{i+1}^n - 2c_i^n + c_{i-1}^n}{(\Delta x)^2}. \tag{32}$$

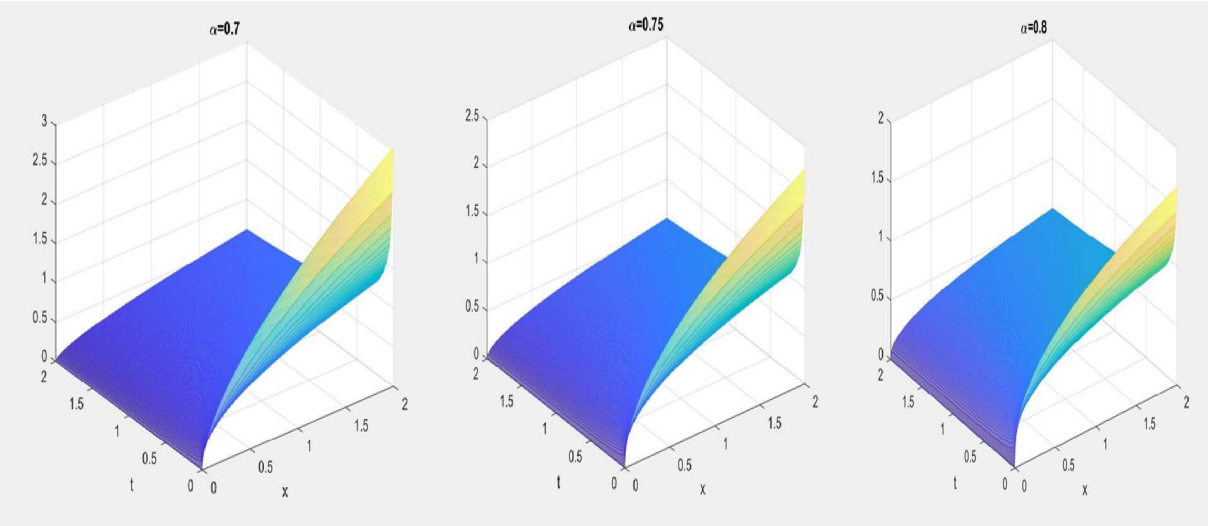

Fig. 3: Numerical simulations of $D(x,t)$ for $\alpha = 0.7$, $\alpha = 0.75$ and $\alpha = 0.8$.

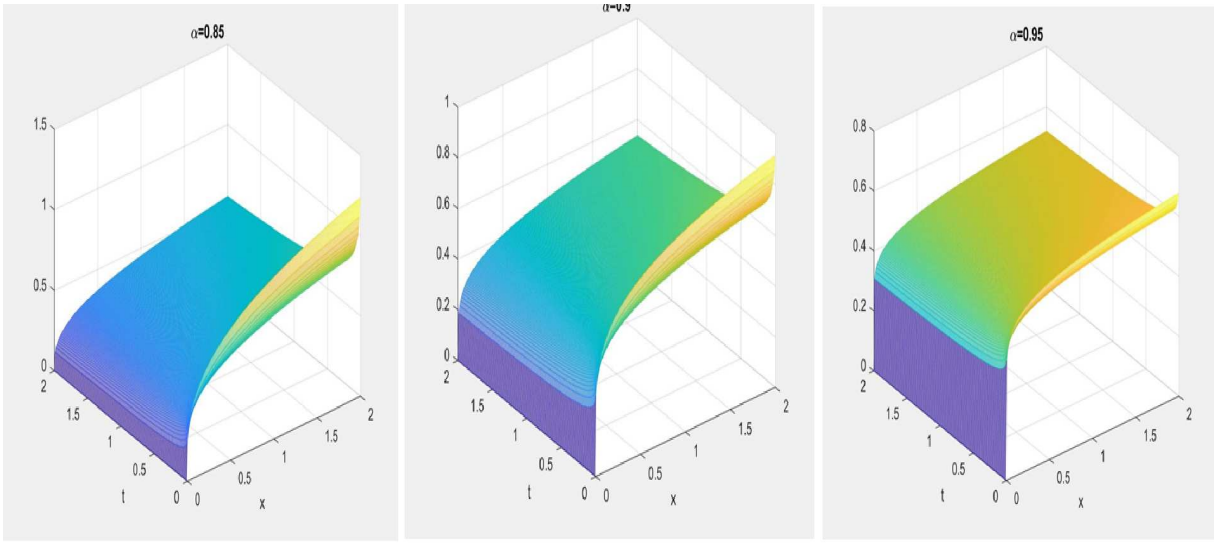

Fig. 4: Numerical simulations of $D(x,t)$ for $\alpha = 0.85$, $\alpha = 0.9$ and $\alpha = 0.95$.

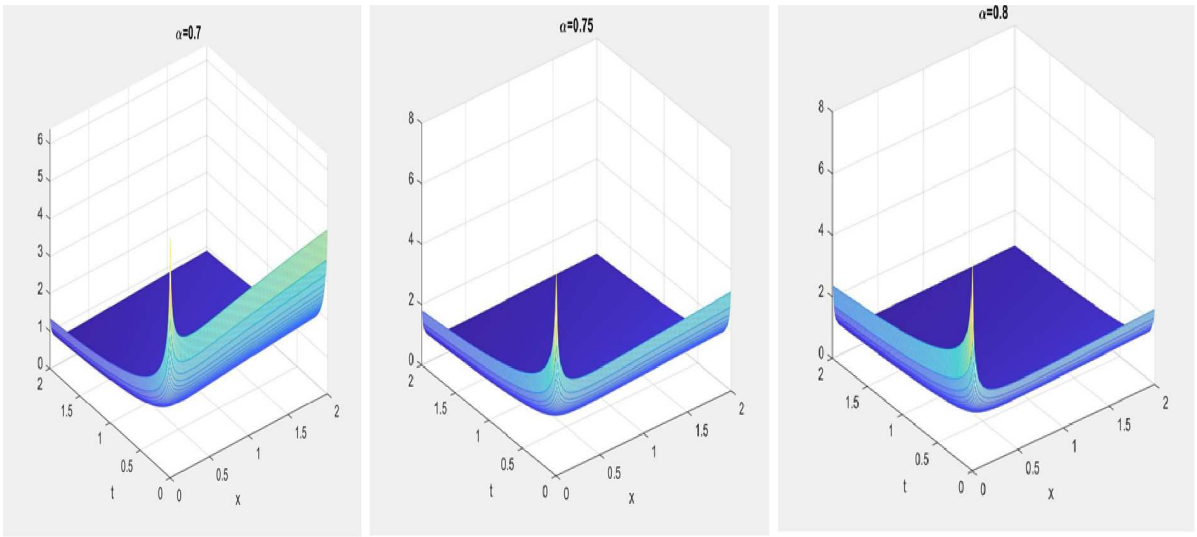

Fig. 5: Numerical simulations of $V(x,t)$ for $\alpha = 0.7$, $\alpha = 0.75$ and $\alpha = 0.8$.

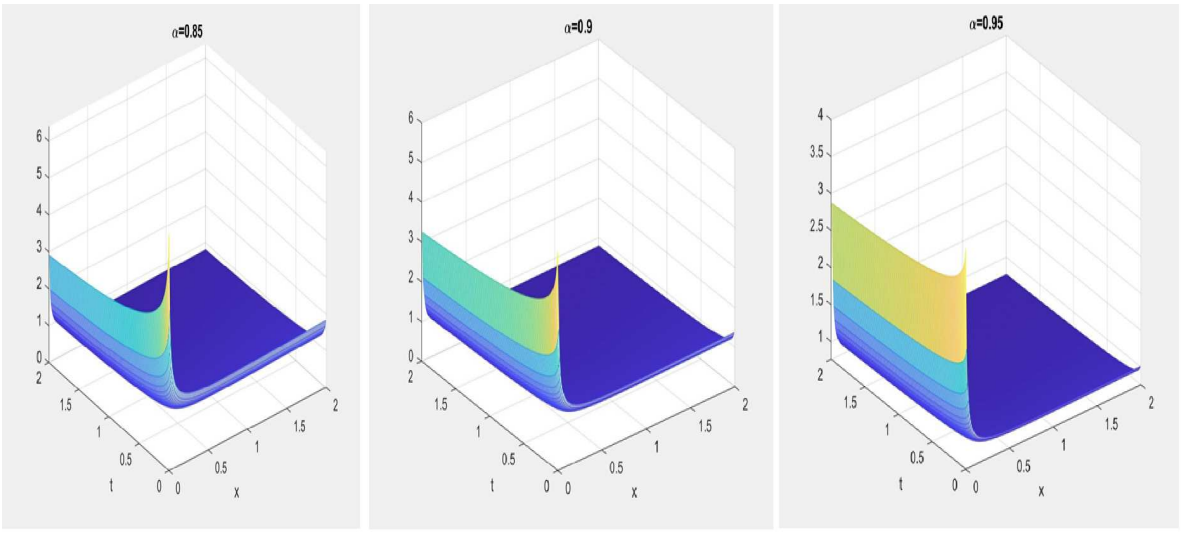

Fig. 6: Numerical simulations of $V(x,t)$ for $\alpha = 0.85$, $\alpha = 0.9$ and $\alpha = 0.95$.

4 Cauchy problem with conformable derivative

We consider in this section a Cauchy problem with conformable derivative.

$$\begin{cases} {}^{\alpha}T_t y(t) = f(t,y(t)), \quad t > 0, \\ y(0) = y_0. \end{cases}$$

We assume that $f(t,y(t))$ is twice differentiable on $(0,T]$. We assume that $y(t)$ is classical differentiable. Thus the above is converted to

$$\begin{cases} \frac{dy(t)}{dt} = t^{\alpha-1} f(t,y(t)), \quad t > 0, \\ y(0) = y_0. \end{cases}$$

$$\begin{cases} y(t) - y(0) = \int_0^t \tau^{\alpha-1} f(\tau,y(\tau)) d\tau, \\ y(0) = y_0. \end{cases}$$

We defined a mapping

$$\Gamma y(t) = y(0) + \int_0^t \tau^{\alpha-1} f(\tau,y(\tau)) d\tau.$$

We defined the following norm

$$\|\phi\|_{\infty} = \sup_{t\in(0,T]} |\phi(t)|.$$

We also assume that $\forall t \in (0,T]$

$$\|f(.,y)\|_{\infty} < M,$$

$$\left\| \frac{\partial^2}{\partial \tau^2} f(.,y) \right\|_\infty < M_1,$$

$$\begin{aligned} |\Gamma y(t) - y_0| &= \left| \int_0^t \tau^{\alpha-1} f(\tau, y(\tau)) d\tau \right|, \\ &\leq \int_0^t \tau^{\alpha-1} |f(\tau, y(\tau))| \, d\tau, \\ &\leq \int_0^t \tau^{\alpha-1} \sup_{l\in[0,\tau]} |f(l, y(l))| \, d\tau, \\ &\leq \sup_{t\in[0,T]} |f(t, y(t))| \frac{T^\alpha}{\alpha}, \\ &< \frac{MT^\alpha}{\alpha}. \end{aligned}$$

We wish to have $\frac{MT^\alpha}{\alpha} < b \quad \Longrightarrow \left(\frac{b\alpha}{M}\right)^{\frac{1}{\alpha}} > T.$

$$\begin{aligned} |\Gamma y_1(t) - \Gamma y_2(t)| &\leq \int_0^t \tau^{\alpha-1} |f(\tau, y_1) - f(\tau, y_2)| \, d\tau, \\ &\leq \int_0^t \tau^{\alpha-1} sup_{l\in[0,\tau]} |f(l, y_1) - f(l, y_2)| \, d\tau. \end{aligned}$$

Using the fact that Lipschitz with L as constant, then we have

$$|\Gamma y_1(t) - \Gamma y_2(t)| \leq \|y_1(t) - y_2(t)\|_\infty L \frac{T^\alpha}{\alpha}.$$

To have a contraction, we wish to have

$$L\frac{T^\alpha}{\alpha} < 1 \quad \Longrightarrow T < \left(\frac{\alpha}{L}\right)^{\frac{1}{\alpha}}.$$

The Cauchy problem with conformable derivative has a unique solution if

$$\max\left(\left(\frac{b\alpha}{M}\right)^{\frac{1}{\alpha}}, \left(\frac{\alpha}{L}\right)^{\frac{1}{\alpha}} \right) < 1.$$

We now present numerical schemes that could be used to solve nonlinear Cauchy problem with conformable derivative.

$$0 < t_1 < t_2 < t_3 < t_4 < ... < t_n = T,$$

$$\begin{aligned} y(t_{n+1}) - y(0) &= \int_0^{t_n} \tau^{\alpha-1} f(\tau, y(\tau)) d\tau, \\ &= \sum_{j=1}^{n} \int_{t_j}^{t_{j+1}} \tau^{\alpha-1} f(\tau, y(\tau)) d\tau, \end{aligned}$$

within $[t_j, t_{j+1}]$. We approximate

$$\begin{aligned} f(\tau, y(\tau)) &= \frac{\tau - t_{j-1}}{\Delta t} f(t_j, y(t_j)) - \frac{\tau - t_j}{\Delta t} f(t_{j-1}, y(t_{j-1})), \\ &+ \frac{(\tau - t_j)(\tau - t_{j-1})}{2} \frac{\partial^2 f(\tau, y(\tau))}{\partial \tau^2} |_{\tau=\xi} \, . \end{aligned}$$

Then, we obtain

$$y(t_{n+1})-y(0)=\sum_{j=1}^{n}\int_{t_j}^{t_{j+1}}\tau^{\alpha-1}\left(\frac{\tau-t_{j-1}}{\Delta t}f(t_j,y(t_j))-\frac{\tau-t_j}{\Delta t}f(t_{j-1},y(t_{j-1}))\right.$$
$$\left.+\frac{(\tau-t_j)(\tau-t_{j-1})}{2}\frac{\partial^2 f(\tau,y(\tau))}{\Delta\tau^2}\mid_{\tau=\xi}\right)d\tau$$
$$=\sum_{j=1}^{n}\int_{t_j}^{t_{j+1}}\tau^{\alpha-1}\left(\frac{\tau-t_{j-1}}{\Delta t}f(t_j,y(t_j))-\frac{\tau-t_j}{\Delta t}f(t_{j-1},y(t_{j-1}))\right)d\tau$$
$$+R_{\alpha,j}(\xi),$$

where $\left|R_{\alpha,j}(\xi)\right|<\infty$.

$$y(t_{n+1})\approx y(0)+\sum_{j=1}^{n}\left[\frac{f(t_j,y(t_j))}{\Delta t}\left(\frac{t_{j+1}^{\alpha+1}}{\alpha+1}-\frac{t_j^{\alpha+1}}{\alpha+1}\right.\right.$$
$$t_{j-1}\left(\frac{t_{j+1}^{\alpha}}{\alpha}-\frac{t_j^{\alpha}}{\alpha}\right)\Big)-\frac{f(t_{j-1},y(t_{j-1}))}{\Delta t}$$
$$\left.\times\left(\frac{t_{j+1}^{\alpha+1}}{\alpha+1}-\frac{t_j^{\alpha+1}}{\alpha+1}-t_j\left(\frac{t_{j+1}^{\alpha}}{\alpha}-\frac{t_j^{\alpha}}{\alpha}\right)\right)\right].$$

$$R_{\alpha,j}(\xi)=\sum_{j=1}^{n}\int_{t_j}^{t_{j+1}}\tau^{\alpha-1}\frac{(\tau-t_j)(\tau-t_{j-1})}{2}\frac{\partial^2 f(\tau,y(\tau))}{\partial\tau^2}\mid_{\tau=\xi}d\tau.$$

$$\left|R_{\alpha,j}(\xi)\right|<\sum_{j=1}^{n}\int_{t_j}^{t_{j+1}}\tau^{\alpha-1}\frac{(\tau-t_j)(\tau-t_{j-1})}{2}\left|\frac{\partial^2 f(\tau,y(\tau))}{\partial\tau^2}\right|_{\tau=\xi}d\tau$$
$$<\sum_{j=1}^{n}\int_{t_j}^{t_{j+1}}\tau^{\alpha-1}\frac{(\tau-t_j)(\tau-t_{j-1})}{2}\sup_{l\in[0,\tau]}\left|\frac{\partial^2 f(l,y(l))}{\partial l^2}\right|_{l=\xi}d\tau$$
$$<\frac{M_1}{2}\sum_{j=1}^{n}\int_{t_j}^{t_{j+1}}\left[\tau^{\alpha+1}-\tau^{\alpha}\left(t_{j-1}+t_j\right)+t_jt_{j-1}\tau^{\alpha-1}\right]d\tau$$
$$<\frac{M_1}{2}\sum_{j=1}^{n}\left[\frac{t_{j+1}^{\alpha+2}}{\alpha+2}-\frac{t_j^{\alpha+2}}{\alpha+2}-(t_{j-1}+t_j)\right.$$
$$\left.\times\left(\frac{t_{j+1}^{\alpha+1}}{\alpha+1}-\frac{t_j^{\alpha+1}}{\alpha+1}\right)+t_jt_{j-1}\left(\frac{t_{j+1}^{\alpha}}{\alpha}-\frac{t_j^{\alpha}}{\alpha}\right)\right]$$
$$<\frac{M_1}{2}(\Delta t)^{\alpha+2}\sum_{j=1}^{n}\left[\frac{(j+1)^{\alpha+2}}{\alpha+2}-\frac{j^{\alpha+2}}{\alpha+2}-(2j-1)\right.$$
$$\left.\times\left(\frac{(j+1)^{\alpha+1}}{\alpha+1}-\frac{j^{\alpha+1}}{\alpha+1}\right)+j(j-1)\left(\frac{(j+1)^{\alpha}}{\alpha}-\frac{j^{\alpha}}{\alpha}\right)\right].$$

However

$$\sum_{j=1}^{n}\left[\frac{(j+1)^{\alpha+2}}{\alpha+2}-\frac{j^{\alpha+2}}{\alpha+2}-(2j-1)\right.,$$
$$\left.\times\left(\frac{(j+1)^{\alpha+1}}{\alpha+1}-\frac{j^{\alpha+1}}{\alpha+1}\right)+j(j-1)\left(\frac{(j+1)^{\alpha}}{\alpha}-\frac{j^{\alpha}}{\alpha}\right)\right],$$

$$\sum_{j=1}^{n}\left[\frac{(j+1)^{\alpha+2}}{\alpha+2}-\frac{j^{\alpha+2}}{\alpha+2}\right]=\frac{1}{\alpha+2}\left((n+1)^{\alpha+2}-1\right),$$

$\forall j\geq 1,\ 2j-1\geq 1\ \longrightarrow -1\geq -(2j-1)$. Thus, we have

$$-\left(\frac{(j+1)^{\alpha+1}}{\alpha+1}-\frac{j^{\alpha+1}}{\alpha+1}\right)\geq -(2j-1)\left(\frac{(j+1)^{\alpha+1}}{\alpha+1}-\frac{j^{\alpha+1}}{\alpha+1}\right),$$

$$\sum_{j=1}^{n}\left(\frac{j^{\alpha+1}}{\alpha+1}-\frac{(j+1)^{\alpha+1}}{\alpha+1}\right)\geq\sum_{j=1}^{n}(1-2j)\left(\frac{(j+1)^{\alpha+1}}{\alpha+1}-\frac{j^{\alpha+1}}{\alpha+1}\right),$$

$$\frac{n^{\alpha+1}-1}{\alpha+1}\geq\sum_{j=1}^{n}(1-2j)\left(\frac{(j+1)^{\alpha+1}}{\alpha+1}-\frac{j^{\alpha+1}}{\alpha+1}\right).$$

We have $\forall j(j-1)\leq n(n-1)\,\forall 1\leq j\leq n$. Thus, we obtain

$$j(j-1)\left(\frac{(j+1)^{\alpha+1}}{\alpha+1}-\frac{j^{\alpha+1}}{\alpha+1}\right)\leq n(n-1)\left(\frac{(j+1)^{\alpha+1}}{\alpha+1}-\frac{j^{\alpha+1}}{\alpha+1}\right),$$

$$\begin{aligned}\sum_{j=1}^{n}j(j-1)\left(\frac{(j+1)^{\alpha}}{\alpha}-\frac{j^{\alpha}}{\alpha}\right)&\leq\sum_{j=1}^{n}j(j-1)\left(\frac{(j+1)^{\alpha}}{\alpha}-\frac{j^{\alpha}}{\alpha}\right)\\&\leq\frac{n(n-1)}{\alpha}\left((n+1)^{\alpha}-1\right).\end{aligned}$$

Therefore, we obtain

$$\begin{aligned}&\sum_{j=1}^{n}\left[\frac{(j+1)^{\alpha+2}}{\alpha+2}-\frac{j^{\alpha+2}}{\alpha+2}-(2j-1)\right.\\&\left.\times\left(\frac{(j+1)^{\alpha+1}}{\alpha+1}-\frac{j^{\alpha+1}}{\alpha+1}\right)+j(j-1)\left(\frac{(j+1)^{\alpha}}{\alpha}-\frac{j^{\alpha}}{\alpha}\right)\right]\\&\leq\frac{1}{\alpha+2}\left((n+1)^{\alpha+2}-1\right)+\frac{1}{\alpha+1}\left((n+1)^{\alpha+1}-1\right)+\frac{n(n-1)}{\alpha}\left((n+1)^{\alpha}-1\right),\end{aligned}$$

$$R_{\alpha,n}(\xi)<\frac{M_1}{2}(\Delta t)^{\alpha+2}\left(\frac{(n+1)^{\alpha+2}-1}{\alpha+2}+\frac{(n+1)^{\alpha+1}-1}{\alpha+1}+\frac{(n+1)^{\alpha}-1}{\alpha}\right).$$

4.1 Generalization

We have shown above that

$$T_t^{\alpha}f(t)=\lim_{t_1\to t}\frac{f(t_1)-f(t)}{t_1^{\alpha}-t^{\alpha}},$$

it exists in a family of rate of change of the function $f(t)$ with respect to the family function $f(t,\alpha)=\frac{t^{\alpha}}{\alpha}$, $0<\alpha\leq 1$. This has being generalized very recently as:

$$D_g(t)f(t)=\lim_{t_1\to t}\frac{f(t_1)-f(t)}{g(t_1)-g(t)}$$

under the condition that $g(t) \neq constance$. If both functions are differentiable in the classical way, then

$$D_g(t)f(t) = \frac{f'(t)}{g'(t)}.$$

It was obtained that

$$D_g(t)f(t) = \frac{f'(t)}{g'(t)} = u(t),$$

$$f'(t) = g'(t)u(t),$$

$$f(t) - f(0) = \int_0^t g'(\tau)u(\tau)d\tau,$$

$$\begin{aligned} f(t) &= f(0) + \int_0^t g'(\tau)u(\tau)d\tau \\ &= f(0) + \int_0^t u(\tau)dg(\tau). \end{aligned}$$

These generalizations were called global derivatives. Here the integral is the well-known Riemann–Stieltjes integral. In the case of fractional derivatives the following generalization was suggested [23,24].

$${}_0^R D_t^\alpha f(t) = \frac{1}{\Gamma(1-\alpha)} D_g \int_0^t f(\tau)(t-\tau)^{-\alpha} d\tau,$$

$${}_0^{AB} D_t^\alpha f(t) = \frac{1}{1-\alpha} D_g \int_0^t f(\tau) E_\alpha \left(-\frac{\alpha}{1-\alpha}(t-\tau)^\alpha \right) d\tau,$$

$${}_0^{CF} D_t^\alpha f(t) = \frac{1}{1-\alpha} D_g \int_0^t f(\tau) \exp\left(-\frac{\alpha}{1-\alpha}(t-\tau) \right) d\tau.$$

Under the conditions of existences of above operators, the associated integrals are given as:

$${}_0^R J_g^\alpha f(t) = \frac{1}{\Gamma(\alpha)} \int_0^t f(\tau)(t-\tau)^{\alpha-1} dg(\tau),$$

$${}_0^{AB} J_g^\alpha f(t) = \frac{1-\alpha}{AB(\alpha)} g'(t)f(t) + \frac{\alpha}{AB(\alpha)\Gamma(\alpha)} \int_0^t f(\tau)(t-\tau)^{\alpha-1} dg(\tau),$$

$${}_0^{CF} J_g^\alpha f(t) = (1-\alpha)g'(t)f(t) + \alpha \int_0^t f(\tau) dg(\tau).$$

5 Applications

The main aim of differential operators is to replicate processes display by real world problems observed in nature. While the rate of change is used to explain changes of a given function with respect to the function t, the conformable derivative explains rate of change of function with respect to the function $\frac{t^\alpha}{\alpha}$. Thus, rate of change generated by conformable derivative between two points a and b gives birth to a family of rate that depends on the fractional variable α of course that when such α is 1 we obtain the classical rate of change. In this section, we shall present some applications of conformable derivative in some important real-world problems, including epidemiology, chaos, and image processing. We shall start with example 1 and application of conformable derivative in image enhancement, in example 2, we shall present application to epidemiology and finally an application to chaos.

Example 1(Application to image processing).
The main key in image processing is to build a new mask with high accuracy and efficiency.

- In segmentation, Thamarai et al. [1] formulated a new combination of conformable focus measures, and focus measure operators in finding redundant separate wavelet transform coefficients for improving the image splicing forgery detection. The procedure of image splicing ailments the relaxed of tampered image and causes abnormality in the image features. The spliced regions boundaries are usually blurring to avoid detection. To make use of the blurred information, both conformable focus measures and focus measure operators are utilized to compute the grade of blurring of the tampered regions boundaries for image splicing detection. The communal image data sets are employed to assess the projected technique.
- Dropping denois in images multiplicatively (DIM) has been established and adapted by numerous investigators throughout the past few years. Ibrahim [2] offered a novel procedure to resolve this problem by using the concept of CC. It has been observed that this kind of calculus has compensations because of its formulation includes a controller, which can be employed in different complex difficulties such as DIM. The suggested constructions of CC windows are given by four masks recommending for x and y directions. This technique leads to improve many factors in images analysis such as visual observation and peak signal-to-noise ratio with Root Mean Square Error and measurements. This study indicated that the skillful filtering outcomes are designated high score than some well known filters such as Gaussian filter, Sobel edge filter, Canny edge filter and gray-level co-occurrence matrix.
- The grey prediction models have been improved by Wanli Xie et al. [3] utilizing conformable fractional derivatives. The proposed method indicated a clear and active grey system, with practical cases. These cases are used to establish the cogency of the planned model. Today, the conformable grey model is applied to recognize the Carbon dioxide emissions in 53 countries [4]. The conformable fractional grey system model is also considered by Ma et al. [5]. The authors proposed an algorithm formulated the conformable fractional accumulation and variance, and Brute Force technique is presented to enhance its fractional order. The viability and straightforwardness of the projected algorithm and the Brute Force technique are shown in the mathematical instance. The conformable fractional grey model overtakes the prevailing fractional grey model and the auto regressive system in 1 to 3 step forecasts with many standard data sets. Moreover, it overtakes the remaining fractional grey model in forecasting the natural gas ingesting of eleven countries. The consequences specify that the planned conformable fractional grey model is additional efficient in longer-term forecast and non-smooth time series estimating than the present simulations.
- Image edge detection is studied widely using fractional calculus in general and CC in particular. CC proved its accursed results in the medical imaging. Lavin-Delgado et al. [6] showed the affectedness of the CC in their book. They formulated an original fractional conformable edge detector for medical image constructions is projected. The suitcases of training are detection and analysis of cerebral arteriovenous deformities, meningioma and medulloblastomas.
- Kumar et al. [7] generalized the Welk-diffusion model, which is used in image denoising. The recommended system is very well-organized for noise elimination of the noisy images in comparison to the classical anisotropic diffusion system. The mathematical experimentation are achieved utilizing an obvious organization for various models of arbitrary calculus. The investigation outcomes are indicated in positions of peak signal to noise ratio as a metric.
- In optic, the extended direct algebraic technique is applied to examine the complex trigonometric and hyperbolic function solutions, particularly dark, singular, collective dark-bright, collective singular, collective dark-singular, collective bright-singular solitons and periodic-singular explanations are indicated of the conformable space-time fractional Fokas-Lenells equation. The existence principles for these explanations are formulated in [8,9,10,11].
- The non-homogeneous grey system is systematically studied in view of the descriptions of the conformable fractional accumulation and difference. The closed-form explanations of the new ideal are discussed by applying mathematical tools and grey theory [12,13].

The characteristics of the fractional conformable derivative, represents the control term of the image by using the fractional parameter. Therefore, the fractional conformable derivative is the only operator that improving the illumination

value of the pixels of the image. Based on the above clime, next we illustrate an experiment result of image analysis by using a conformable mask, which is given by the approximated solutions of a conformable heat equation [18], as follows:

$$\begin{aligned}\varphi_1 &\approx \frac{4}{\alpha(3-\alpha)\Gamma(1+\alpha)},\\ &\vdots\\ \varphi_n &\approx \frac{(n+1)\Gamma(n+2)\Gamma(\alpha)\Gamma(3-\alpha)}{\Gamma(n+\alpha)\Gamma(n+3-\alpha)}.\end{aligned}$$

Or by utilizing the 2D-conformable mask [2] with the formula

$$\sigma^{\alpha}(i,j) = \frac{1}{\Gamma(i+j-\alpha)},$$

where the pair (i,j) indicates the 2D-position of the pixel. Our window is suggested by using one of the following 3×3 dimensional matrix

$$\Phi_0 = \begin{pmatrix} 0 & 0 & 0\\ \varphi_1 & \varphi_2 & \varphi_3\\ 0 & 0 & 0\end{pmatrix}, \quad \Phi_{45^o} = \begin{pmatrix} 0 & 0 & \varphi_1\\ 0 & \varphi_2 & 0\\ \varphi_3 & 0 & 0\end{pmatrix}$$
$$\Phi_{90^o} = \begin{pmatrix} 0 & \varphi_1 & 0\\ 0 & \varphi_2 & 0\\ 0 & \varphi_3 & 0\end{pmatrix}, \quad \Phi_{135^o} = \begin{pmatrix} \varphi_1 & 0 & 0\\ 0 & \varphi_2 & 0\\ 0 & 0 & \varphi_3\end{pmatrix}.$$

This part presents the results of image enhancement model using conformable mask. The results of three different images in Figures 7-10 illustrate the comparison between conformable mask and classical derivative image enhancement.

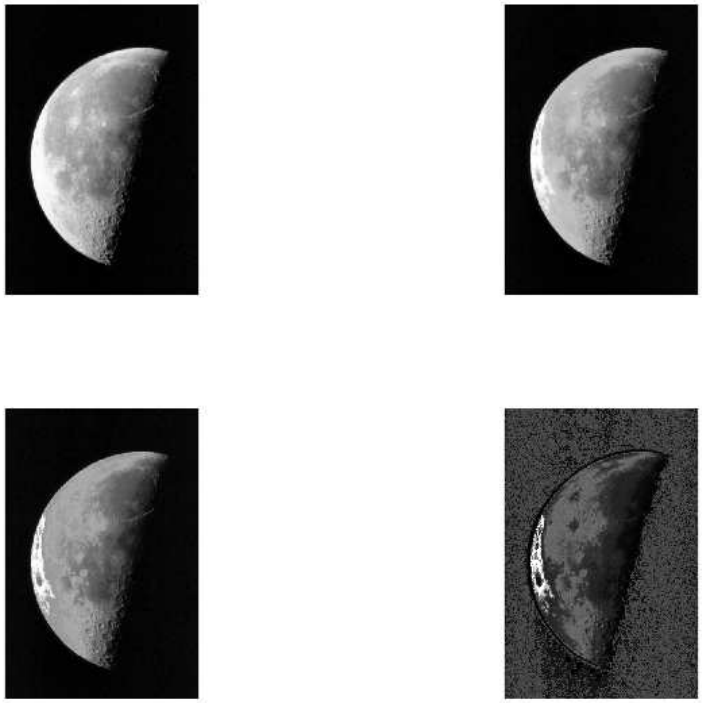

Fig. 7: Image of Moon. First row: input image, and output image with α=0.2 Second row: output image with α=0.25, and output image with α=1

Fig. 8: Image of Cameraman. First row: input image, and output image with α=0.2 Second row: output image with α=0.25, and output image with α=1

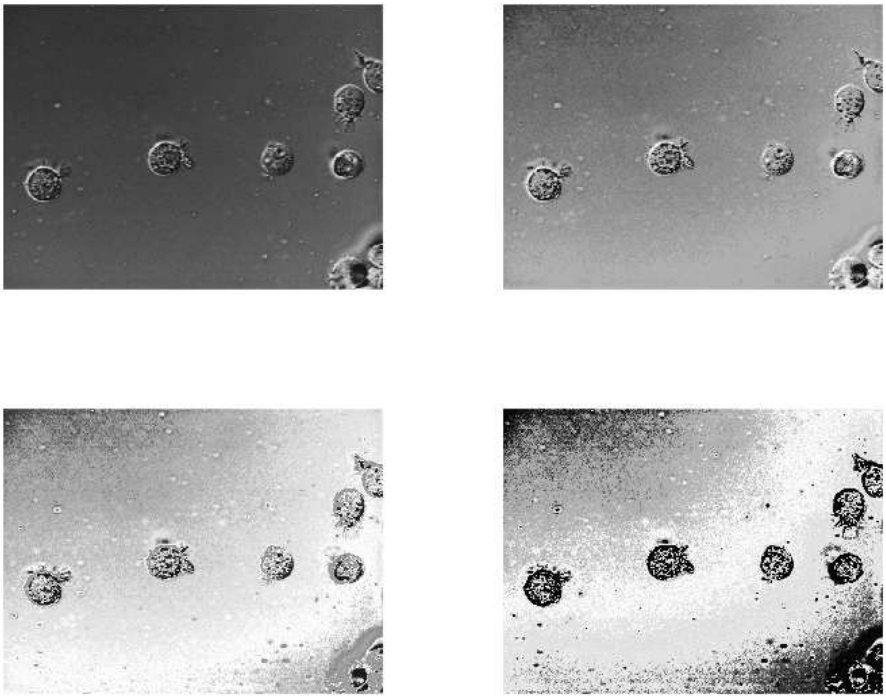

Fig. 9: Image Biological Cells. First row: input image, and output image with α=0.2 Second row: output image with α=0.25, and output image with α=1

Table 1: The quality quantitative results for enhanced images with different values of the parameter α

Enhanced Image(α=1)		α= 0.1	α= 0.25	α= 1
The Moon	BRISQUE	23.4415	21.6535	37.6467
	PIQE	24.3316	20.9617	54.9856
Cameraman	BRISQUE	10.7943	34.5127	37.6380
	PIQE	43.2586	49.1233	50.1359
Biological cells	BRISQUE	32.6612	31.9820	36.0930
	PIQE	24.0358	38.5541	50.1932
African Fractional Man	BRISQUE	30.4273	30.1715	36.1337
	PIQE	51.5667	53.4415	60.2312

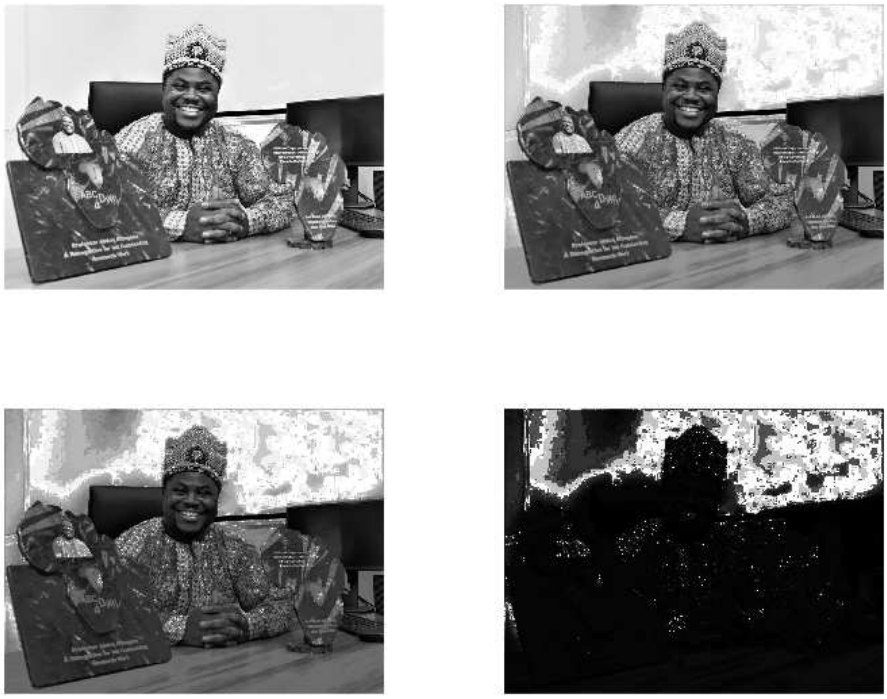

Fig. 10: African Fractional Man [21]. First row: input image, and output image with α=0.1 Second row: output image with α=0.25, and output image with α=1

To evaluate the proposed image enhancement model, we use two no-reference image quality assessment metrics, which are:

(i)"The blind reference-less image spatial quality evaluator (Brisque)", which calculates the perceptual quality of images [19].
(ii)"Perception based image quality evaluator (Piqe)", which calculates the image quality affected by arbitrary distortion [20]

The achieved quality quantitative results of the enhancement images are stated in Table 1. Most of the image enhancement methods reported in the literature use the no reference image quality metrics, therefore, the Brisque and Piqe scores have been used for the quantitative comparisons as presented in Table 1. It is noted from Table 1 that lower scores of Brisque, and Piqe indicate better quality of the enhanced images when α= 0.25. However, when α=1, represents the classic derivative, the Brisque, and Piqe indicate the lowest image quality among other conformable fractional power α.

Example 2(Application to epidemiological).

The classical model suggested by [14] for the transmission dynamics of dengue fever. The humans populations is divided into three components that are, the susceptible individuals (that easily attract the disease), $S_h(t)$, individuals infected after biting by the mosquitos is $I_h(t)$, individuals recovered or removed from infection is given by $R_h(t)$. So, we can denote the total population of humans by $N_h(t)$ and $N_h(t) = S_h(t) + I_h(t) + R_h(t)$. The population of mosquitoes denoted by $N_m(t)$ and it is dividend further into $S_m(t)$ and $I_m(t)$, respectively denote the susceptible and infected mosquitoes. So, $N_m(t) = S_m(t) + I_m(t)$. The classical model that governs the system of nonlinear evolutionary differential

equations is given by the system below:

$$\begin{cases} \frac{\mathrm{dS_h}}{\mathrm{d}t} = \mu_\mathrm{h}\left(N_\mathrm{h} - S_\mathrm{h}\right) - \frac{\beta_\mathrm{h} b}{N_\mathrm{h}+m} S_\mathrm{h} I_\mathrm{m} \\ \frac{\mathrm{d}I_\mathrm{h}}{\mathrm{d}t} = \frac{\beta_\mathrm{h} b}{N_\mathrm{h}+m} S_\mathrm{h} I_\mathrm{m} - \left(\mu_\mathrm{h} + \gamma\right) I_\mathrm{h} \\ \frac{\mathrm{d}R_\mathrm{h}}{\mathrm{d}t} = \gamma I_\mathrm{h} - \mu_\mathrm{h} R_\mathrm{h} \\ \frac{\mathrm{d}S_\mathrm{m}}{\mathrm{d}t} = \Lambda - \frac{\beta_\mathrm{m} b}{N_\mathrm{h}+m} S_\mathrm{m} I_\mathrm{h} - \mu_\mathrm{m} S_\mathrm{m} \\ \frac{\mathrm{d}I_\mathrm{m}}{\mathrm{d}t} = \frac{\beta_\mathrm{m} b}{N_\mathrm{h}+m} S_\mathrm{m} I_\mathrm{h} - \mu_\mathrm{m} I_\mathrm{m}, \end{cases} \tag{33}$$

with nonnegative initial conditions

$$S_h(0) = S_0^h,\ I_h(0) = I_0^h,\ R_h(0) = R_0^h,\ S_m(0) = S_0^m,\ I_m(0) = I_0^m. \tag{34}$$

In above system, the natural death rate of humans and mosquitoes are given by μ_h and μ_m. The recovery rate of infected people is shown by γ, the biting rate by b, m denotes the number of alternative blood sources available to the mosquitoes other than humans. The constant rate of recruitment of the mosquitoes population is given by Λ. The transmission probability from human to mosquitoes and misquotes to humans are given by β_m and β_h.
We can observe by adding the first three equations of the model (33) given by

$$\begin{aligned} \frac{dN_h}{dt} &= \frac{\mathrm{dS_h}}{\mathrm{d}t} + \frac{\mathrm{dR_h}}{\mathrm{d}t} + \frac{\mathrm{d}I_\mathrm{h}}{\mathrm{d}t}, \\ &= \mu_\mathrm{h}\left(N_\mathrm{h} - S_\mathrm{h} - I_\mathrm{h} - R_\mathrm{h}\right) = 0, \end{aligned} \tag{35}$$

which describes that the population is constant. Similarly, we can add the last two equations of the model (33), and have

$$\begin{aligned} \frac{\mathrm{d}N_\mathrm{m}}{\mathrm{d}t} &= \frac{\mathrm{dS_m}}{\mathrm{d}t} + \frac{\mathrm{d}I_\mathrm{m}}{\mathrm{d}t}, \\ &= \Lambda - \mu_\mathrm{m}\left(S_\mathrm{m} + I_\mathrm{m}\right) \\ &= \Lambda - \mu_\mathrm{m} N_\mathrm{m}. \end{aligned} \tag{36}$$

We consider the real cases of dengue fever outbreak reported in Cape Verde islands in 2009, see for more details [14,15]. We aim to provide the good fitting to the real cases using the model (33) by considering the conformable derivative. First, we replace the model as suggested by [15], which takes the following form:

$$\begin{cases} \frac{\mathrm{dS_h}}{\mathrm{d}t} = \mu_\mathrm{h}\left(N_\mathrm{h} - S_\mathrm{h}\right) - \frac{\beta_\mathrm{h} b}{N_\mathrm{h}} S_\mathrm{h} I_\mathrm{m} \\ \frac{\mathrm{d}I_\mathrm{h}}{\mathrm{d}t} = \frac{\beta_\mathrm{h} b}{N_\mathrm{h}} S_\mathrm{h} I_\mathrm{m} - \left(\mu_\mathrm{h} + \gamma\right) I_\mathrm{h} \\ \frac{\mathrm{d}R_\mathrm{h}}{\mathrm{d}t} = \gamma I_\mathrm{h} - \mu_\mathrm{h} R_\mathrm{h} \\ \frac{\mathrm{d}S_\mathrm{m}}{\mathrm{d}t} = \mu_m N_m - \frac{\beta_\mathrm{m} b}{N_\mathrm{h}} S_\mathrm{m} I_\mathrm{h} - \mu_\mathrm{m} S_\mathrm{m} \\ \frac{\mathrm{d}I_\mathrm{m}}{\mathrm{d}t} = \frac{\beta_\mathrm{m} b}{N_\mathrm{h}} S_\mathrm{m} I_\mathrm{h} - \mu_\mathrm{m} I_\mathrm{m}. \end{cases} \tag{37}$$

The model (37) in the sense of conformable derivative as given in [16], can be written as

$$\begin{cases} T_\alpha(S_h(t)) = t^{\alpha-1}[\mu_\mathrm{h}\left(N_\mathrm{h} - S_\mathrm{h}\right) - \frac{\beta_\mathrm{h} b}{N_\mathrm{h}} S_\mathrm{h} I_\mathrm{m}] \\ T_\alpha(I_h(t)) = t^{\alpha-1}[\frac{\beta_\mathrm{h} b}{N_\mathrm{h}} S_\mathrm{h} I_\mathrm{m} - \left(\mu_\mathrm{h} + \gamma\right) I_\mathrm{h}] \\ T_\alpha(R_h(t)) = t^{\alpha-1}[\gamma I_\mathrm{h} - \mu_\mathrm{h} R_\mathrm{h}] \\ T_\alpha(S_m(t)) = t^{\alpha-1}[\mu_m N_m - \frac{\beta_\mathrm{m} b}{N_\mathrm{h}} S_\mathrm{m} I_\mathrm{h} - \mu_\mathrm{m} S_\mathrm{m}] \\ T_\alpha(I_m(t)) = t^{\alpha-1}[\frac{\beta_\mathrm{m} b}{N_\mathrm{h}} S_\mathrm{m} I_\mathrm{h} - \mu_\mathrm{m} I_\mathrm{m}]. \end{cases} \tag{38}$$

We written $T_\alpha()$ to denote the conformable fractional derivative of f of order α. Also, we write the system (38) in the following form:

$$\begin{cases} T_\alpha(S_h(t)) = t^{\alpha-1}[\mu_{\rm h}^\alpha(N_{\rm h}-S_{\rm h}) - \frac{\beta_{\rm h}b^\alpha}{N_{\rm h}}S_{\rm h}I_{\rm m}] \\ T_\alpha(I_h(t)) = t^{\alpha-1}[\frac{\beta_{\rm h}b^\alpha}{N_{\rm h}}S_{\rm h}I_{\rm m} - (\mu_{\rm h}^\alpha+\gamma^\alpha)I_{\rm h}] \\ T_\alpha(R_h(t)) = t^{\alpha-1}[\gamma^\alpha I_{\rm h} - \mu_{\rm h}^\alpha R_{\rm h}] \\ T_\alpha(S_m(t)) = t^{\tau-1}[\mu_m^\tau N_m - \frac{\beta_{\rm m}b^\tau}{N_{\rm h}}S_{\rm m}I_{\rm h} - \mu_{\rm m}^\tau S_{\rm m}] \\ T_\alpha(I_m(t)) = t^{\tau-1}[\frac{\beta_{\rm m}b^\tau}{N_{\rm h}}S_{\rm m}I_{\rm h} - \mu_{\rm m}I_{\rm m}^\tau]. \end{cases} \tag{39}$$

When α and τ approaches 1 in system (39), then we have the classical model. The model (39) solution numerically with data comparison, we show in the next and will be the best model for fitting to the outbreak data. We will compare the models (37, 38, 39) with real data and the same parameters values will be considered together with initial values of the variables.

We consider the initial values of the model variables suggested by [15]: $S_h(0) = 55784$, $I_h(0) = 216$, $R_h(0) = 0$, $S_m(0) = 168000$ and $I_m(0) = 0$. The parameters values as given in [15] are $\mu_h = \frac{1}{71.365}$, $\mu_m = 0.1$, $\beta_h = \beta_m = 0.36$, $b = 0.7$ and $\gamma = 1/3$. The real outbreak data has been plotted in Figure 11. The classical model (37) and its comparison with the outbreak data is shown in Figure 12, where one can observe that the model is poorly fitted to the data. Comparison of the classical model (37) and the fractional conformable derivative model (38) with real data is shown in Figure 13. We can see that the fractional order model (38) provides better result to the data as compared to the classical model (37). We give comparison of the model (39) and classical model (37) with real data shown in Figure 14. The sub-graph (a) in Figure 14 shows that the that fractional model (39) formulated using conformable derivative provides better fitting to the real data as compared to the classical model (37). To see the better view of the fractional model (39) with real data, we have Figure 5 (b). The results provides in this work for the comfortable derivative and its application to the outbreak data of dengue fever is useful and no one can neglect the importance of conformable derivative to real data fitting. Any one can confidently apply the conformable derivative to other real data problems arising from science and engineering field. We can highlight here that the results suggested by [15] for the outbreak model of dengue fever in terms of fractional Caputo case were better than the previous work. In comparison to the work in [15], our results are better.

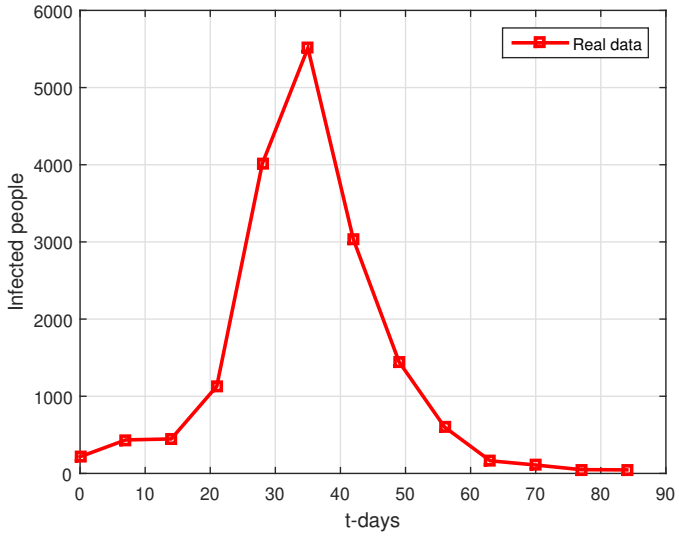

Fig. 11: The outbreak cases in the 2009 Cape Verde.

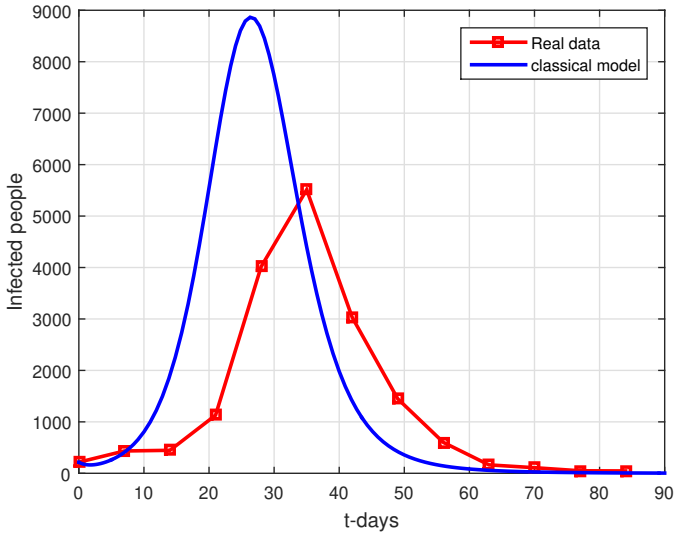

Fig. 12: Comparison of classical model (37) with real data.

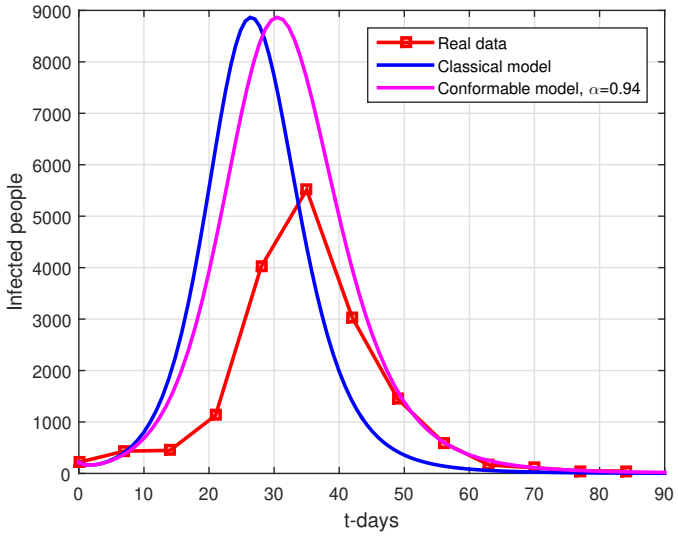

Fig. 13: Comparison of classical model (37), fractional conformable model (38) with real data.

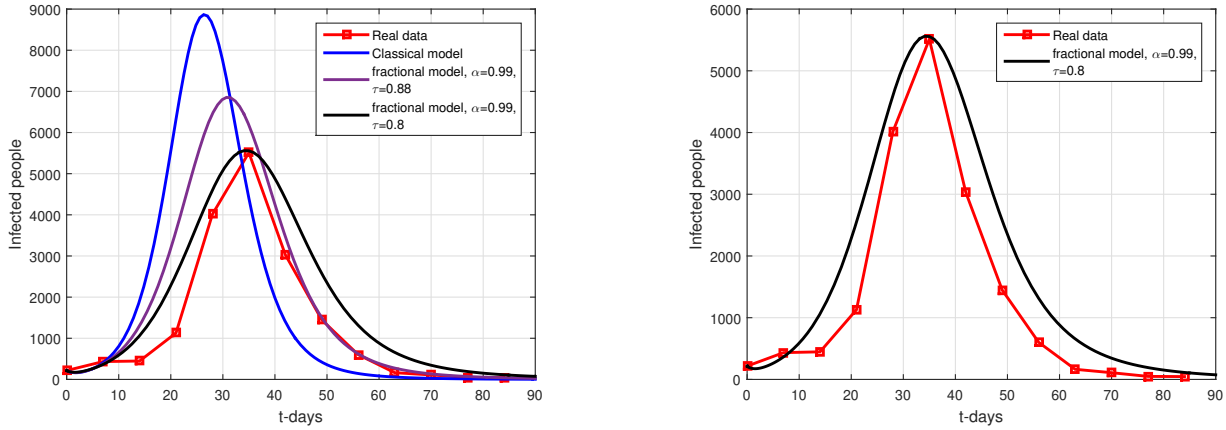

fig:subfig2

Fig. 14: Comparison of models with real data: (a) describes the comparison of model (39) and classical model (37) with real data while (b) is the explicit figure for comparison of model (39) with real data.

Example 3(Application to chaos). Here we consider the chaotic problem presented in [17]. The system is presented through the following nonlinear system:

$$\begin{cases} \dot{x} = a(y-x), \\ \dot{y} = (c-a)x - xz + cy, \\ \dot{z} = xy - bz, \end{cases} \tag{40}$$

Using the definition of conformable derivative, we have the system (40) like this

$$\begin{cases} T_\alpha(x(t)) = a(y-x), \\ T_\alpha(y(t)) = (c-a)x - xz + cy, \\ T_\alpha(z(t)) = xy - bz. \end{cases} \tag{41}$$

The systems (41,40) are chaotic for $a = 35,\ c = 28, b = 3$ with the initial values of state variables $x(0) = -10$, $y(0) = 0$ and $z(0) = 37$. Figure 15 demonstrates that the system is chaotic. Figures 16-18 describe the simulation of the model (41) for different α's.

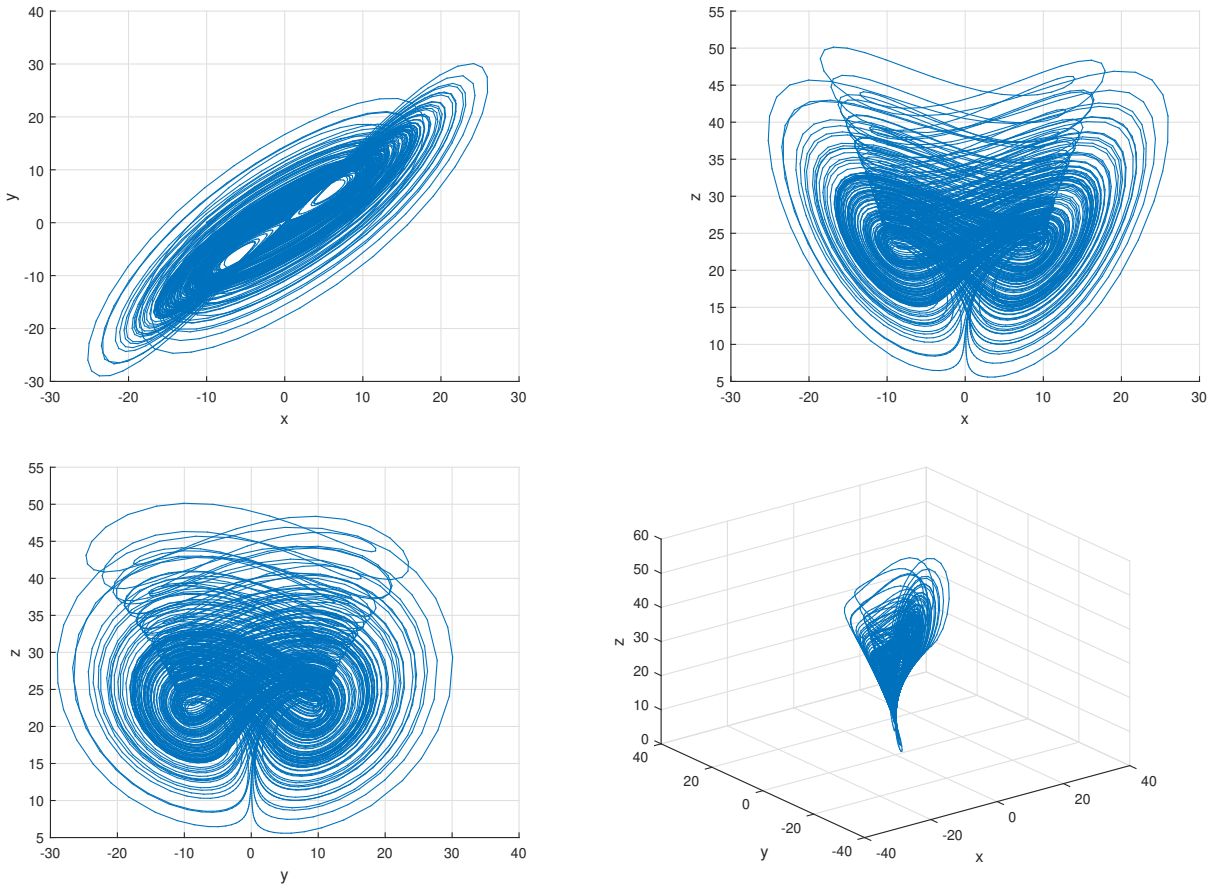

Fig. 15: Simulation of fractional chaotic system (41) for $\alpha = 1$, and $t \in [0, 100]$.

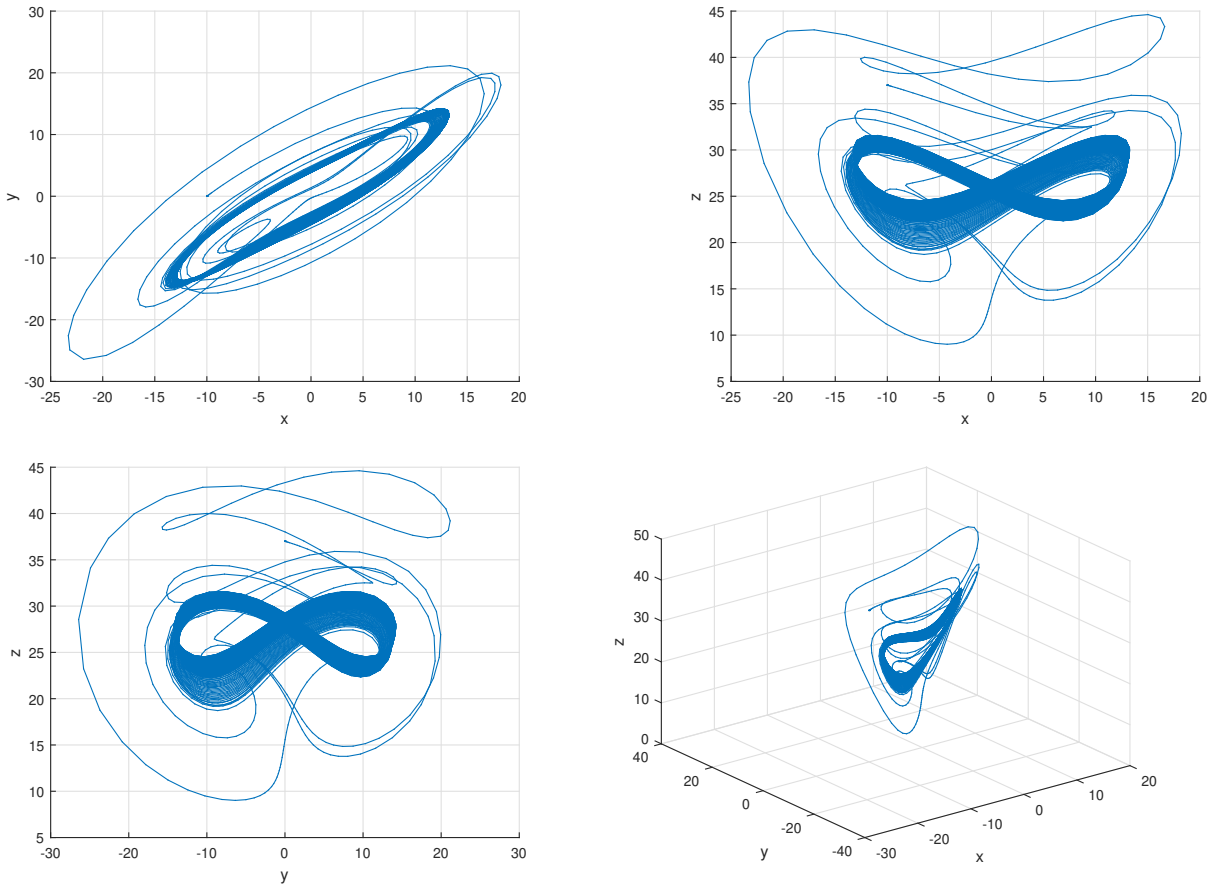

Fig. 16: Simulation of fractional chaotic system (41) for $\alpha = 0.98$ and $t \in [0, 100]$.

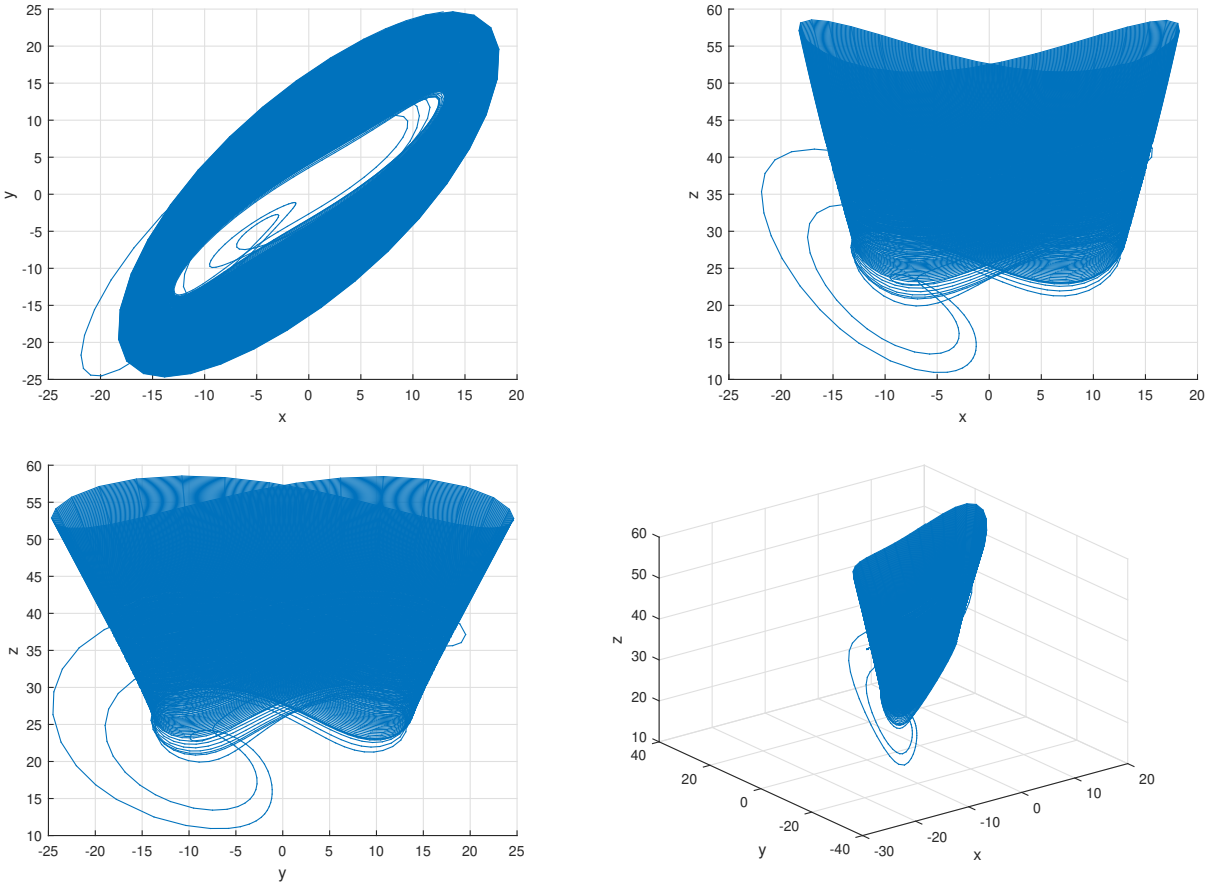

Fig. 17: Simulation of fractional chaotic system (41) for $\alpha = 0.96$ and $t \in [0, 100]$.

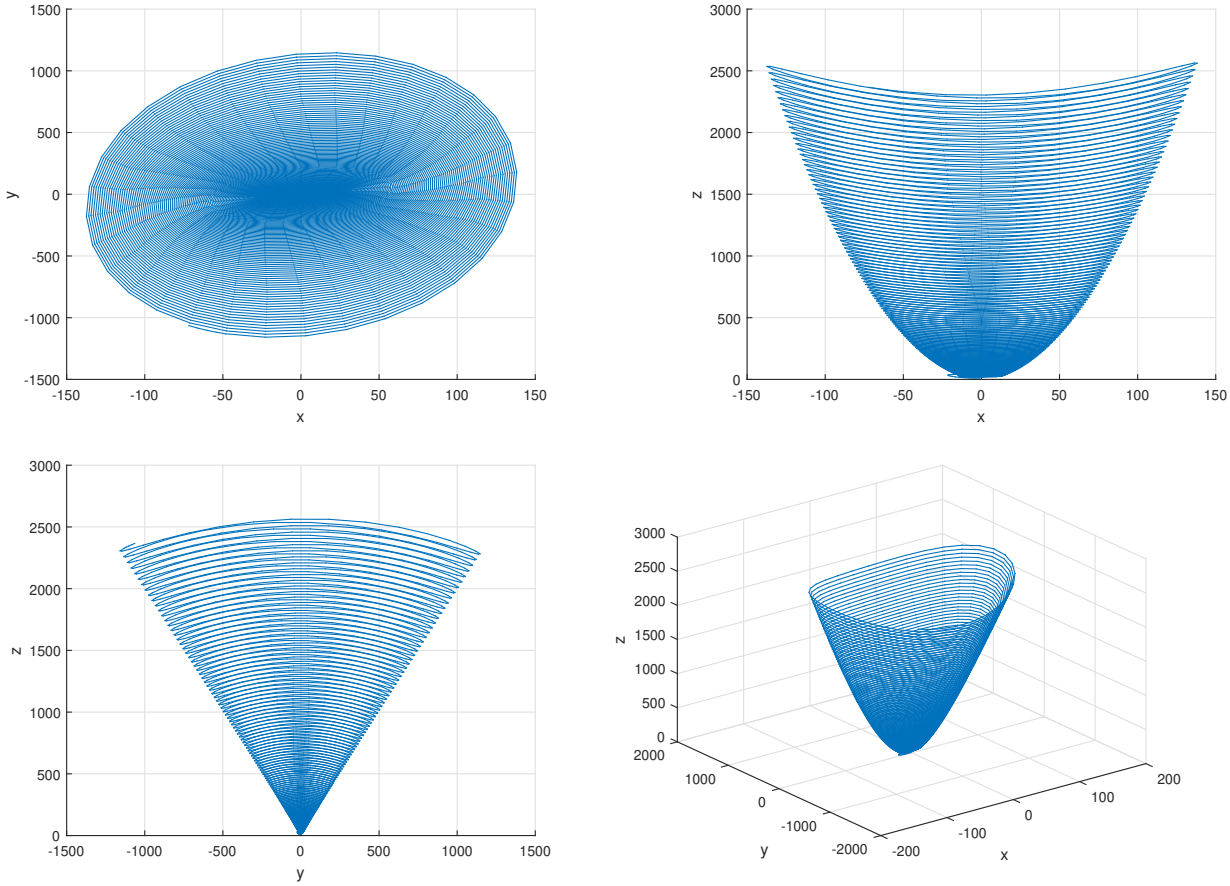

Fig. 18: Simulation of fractional chaotic system (41) for $\alpha = 0.92$ and $t \in [0, 100]$.

6 Conclusion

The aim of this paper was to show that the conformable operator is indeed a derivative with different properties than the classical differential operators. To do this, we considered the well-known Riemann-Stieltjes integral that is well-known to be a more general integral than the classical integral. By choosing a specific function g(t), we obtained a specific class of Riemann-Stieltjes integral, using the fundamental theorem of calculus, we recovered the conformable derivative. It then turns out that, the conformable operator is indeed a more general differential operator that coincides with classical derivative when alpha is 1 and its associate integral is indeed special Riemann-Stieltjes integral. The operator helps evaluate the rate of change of functions with respect to the function $\frac{t^\alpha}{\alpha}$. We proved that, applying conformable derivative to a model with classical derivative lead to an equation with fractal variable coefficients. We applied the operator in more sensitive problems and got complex behaviors that cannot be captured by classical derivative.

Conflicts of Interests

The authors declare that they have no conflicts of interests

References

[1] T. Subramaniam, A. J. Hamid, W. I. Rabha and F. M. N. Nurul, Improved image splicing forgery detection by combination of conformable focus measures and focus measure operators applied on obtained redundant discrete wavelet transform coefficients, *Symmetry* **11**(11), 1392 (2019).

[2] W. I. Rabha, A new image denoising model utilizing the conformable fractional calculus for multiplicative noise. *SN Appl. Sci.* **2**(1), 1-11 (2020).

[3] X. Wanli, C. Liu, W. Z. Wu, W. Li and C. Liu, Continuous grey model with conformable fractional derivative, *Chaos, Solit. Fract.* **139**, 110285 (2020).
[4] X. Zhicun, L. Liu and L. Wu, Forecasting the carbon dioxide emissions in 53 countries and regions using a non-equigap grey model *Environ. Sci. Poll. Res.* **28**(13), 15659-15672 (2021).
[5] M. Xin, W. Wu, B. Zeng, Y. Wang and X. Wu, The conformable fractional grey system model,*Transactions* **96**, 255-271 (2020).
[6] J. E. Lavin-Delgado, J. E. Solis-Perez, J. F. Gomez-Aguilar and R. F. Escobar-Jiménez, Image edge detection using fractional conformable derivatives in Liouville-Caputo sense for medical image processing. *In Fractional Calculus in Medical and Health* Science, pp. 1-54. CRC Press, 2020.
[7] S. Kumar, A. Khursheed and C. Alka, Fractional derivative based nonlinear diffusion model for image denoising, *SEMA J.*, 1-10 (2020).
[8] N. Sajid and A. Ghazala, Optical solitons with full nonlinearity for the conformable space-time fractional Fokas–Lenells equation *Optik* **196**, 163-131 (2019).
[9] J. J. Rosales, F. A. Godínez, V. Banda and G. H. Valencia, Analysis of the Drude model in view of the conformable derivative, *Optik* **178**, 1010-1015 (2019).
[10] K. Wajdi, H. Almusawa, S. M. Mirhosseini-Alizamini, M. Eslami, H. Rezazadeh and M. S. Osman, Optical soliton solutions for the coupled conformable Fokas-Lenells equation with spatio-temporal dispersion *Res. Phys.* 104388 (2021).
[11] H. Amjad, A. Jhangeer, N. Abbas, I. Khan and E. S. M. Sherif, Optical solitons of fractional complex Ginzburg-Landau equation with conformable, beta, and M-truncated derivatives: a comparative study *Adv. Differ. Equ.* **1**, 1-19 (2020).
[12] W. Wenqing, X. Ma, Y. Zhang, W. Li and Y. Wang, A novel conformable fractional non-homogeneous grey model for forecasting carbon dioxide emissions of BRICS countries *Sci. Tot. Env.* **707**, 135447 (2020).
[13] X. Wanli, M. Pang, W. Z. Wu and C. Liu, A framework for general conformable fractional grey system models: a physical perspective and its actual application. arXiv preprint arXiv:2104.01114 (2021).
[14] H. Nishiuraet, Mathematical and statistical analyses of the spread of dengue, (2006).
[15] K. Diethelm, A fractional calculus based model for the simulation of an outbreak of dengue fever, *Nonlinear Dyn.* **71** (4), 613–619 (2013).
[16] R. Khalil, M. Al Horani, A. Yousef and M. Sababheh, A new definition of fractional derivative, *J. Comput. Appl. Math.* **264**, 65–70 (2014).
[17] G. Chen and T. Ueta, Yet another chaotic attractor, *Int. J. Bifur. Chaos,* **9(07)**, 1465–1466 (1999).
[18] R. W. Ibrahim, H. A. Jalab, F. K. Karim, E. Alabdulkreem and M. N. Ayub, A medical image enhancement based on generalized class of fractional partial differential equations, *Quant. Imag. Med. Surg.* 1-12, 2021.
[19] A. Mittal, A. K. Moorthy and A. C. Bovik, Blind/referenceless image spatial quality evaluator. In: 2011 Conference Record of the Forty Fifth Asilomar Conference on Signals, Systems and Computers (ASILOMAR). IEEE, 2011. doi: 10.1109/ACSSC.2011.6190099 (2011).
[20] N. Venkatanath, D. Praneeth, M. C. Bh, S. S. Channappayya and S. S. Medasani, Blind image quality evaluation using perception based features. In: 2015 Twenty First National Conference on Communications (NCC). IEEE, (2015).
[21] B. Ghanbari and A. Atangana, Some new edge detecting techniques based on fractional derivatives with non-local and non-singular kernels, *Adv. Differ. Equ.* **1**, 1-19 (2020).
[22] R. Khalil, A. Al Horani, A. Yousef and M. Sabadheh, A new definition of fractional derivative, *J. Comput. Appl. Math.* **264**, 65-70 (2014).
[23] M. Caputo and M. Fabrizio, A new definition of fractional derivative without singular kernel, *Progr. Fract. Differ. Appl.* **1**(2), 73-85 (2015).
[24] A. Atangana and D. Baleanu, New fractional derivatives with nonlocal and non-singular kernel: theory and application to heat transfer model, *Therm. Sci.* **20 (2)**, 763-769 (2016).